Jovid Rakhmonov[a,b], Giulio Timelli[a], Alberto Fabrizi[a], Franco Bonollo[a]
[a] Department of Management and Engineering, University of Padova, Vicenza, Italy.
[b] Presently: Department of Applied Sciences,University of Quebec at Chicoutimi, Canada

Effect of V and Zr microalloying, and heat treatment on microstructure and mechanical properties of secondary Al-7Si-3Cu-0.3Mg alloy

The Al–Si–Cu alloys, which are widely used in automotive powertrains, exhibit limited high-temperature strength properties; the high diffusivity of the main strengthening elements Cu and Mg in α-Al at temperatures between 200 and 300 °C is a dominating factor in alloy softening. In this study, effects of slow-diffusing elements (Zr and V) and heat treatment on the microstructure and mechanical properties of secondary Al-7Si-3Cu-0.3Mg alloy were investigated. Majorities of both Zr and V were retained inside the α-Al matrix during solidification. T6 heat treatment induced the solid-state precipitation of multiple, nano-sized particles in α-Al grain interiors. Unlike Cu/Mg-rich strengthening precipitates that form during aging, the Zr/V-rich precipitates formed during solution heat treatment, which indicates high potential for high-temperature strengthening in Al–Si alloys via transition metal addition. Other transition metals, such as Mn, Fe, Cr and Ti, which were present as impurities in the base alloy significantly promoted the formation of nano-sized Zr/V-rich precipitates inside α-Al grains. These thermally more stable precipitates were credited for the enhanced high-temperature strength properties of Al-7Si-3Cu-0.3Mg alloy by ∼20 %.

Keywords: Al–Si alloys; Microstructure; Mechanical properties; High-temperature strength; Transition elements.

1. Introduction

Pursuit of light-weight in the automotive industry for fuel efficiency has led to a large-scale application of aluminum alloys. Some engine components, such as cylinder-head and -block, have been increasingly fabricated using Al–Si–Mg or Al–Si–Cu–Mg alloys as these alloys offer a combination of excellent casting characteristics and relatively high mechanical properties [1, 2]. The presence of Cu and/or Mg in the alloy provides significant strengthening by precipitation hardening [3]. However, the Cu/Mg-rich precipitates can only be effective for the strength at temperatures below 200 °C [4]. At higher temperatures, solute diffusion of Cu and Mg tends to be increasingly effective in promoting precipitate coarsening, also called Ostwald ripening, within the matrix, thus contributing to the alloy softening [5]. The operating temperature in the engine combustion chamber can often exceed 200 °C during service [6, 7]. Moreover, a further increase in operating temperature is anticipated due to the expected enhancement in engine power in the near future, which indicates the necessity for the development of new creep-resistant Al alloys [8].

A new alloy must resist degradation of mechanical properties at high temperatures (200 – 300 °C). Addition of some transition metals, such as Sc, Zr, V, Mo, Ni etc. are thought to give this characteristic as these elements have low diffusivity in α-Al at higher temperatures and can form coherent or semi-coherent precipitates in stable and/or meta-stable states [9]. Owing to low solid solubility in α-Al matrix, these transition elements, if added individually, make less contribution to the strengthening of the material due to the limited volume fraction of precipitates forming during heat treatment. Combined addition of appropriate types of transition metals, in contrast, can yield higher volume fraction of precipitates, thus positively influencing the thermal stability of the alloy [9, 10]. Adding transition metals in an effort to improve the high-temperature mechanical properties of Al–Si based alloys has been a research topic of several studies [8, 11–18]. Kasprzak et al. [19] reported how minor Ti, Zr and V additions can yield the formation of nano-sized $(AlSi)_3(ZrVTi)$ precipitates in grain interiors, however, their effect on high-temperature tensile properties has been found to be negligible, which can be due to the limited volume fraction of thermally stable precipitates. Shaha et al. [8] stated how the addition of 0.56 % Zr, 0.3 % V and 0.3 % Ti can improve the low-cycle fatigue properties of Al–Si–Cu–Mg based alloy due to the formation of both interdendritic and intradendritic Zr/V-rich precipitates. However, the addition levels of peritectic-forming elements need optimization as too high levels also lead to the premature nucleation and growth of phases with undesired morphology, thus having a deleterious impact on alloy performance, as observed in Refs. [13, 16]. Farkoosh et al. [20] found how the interaction between the eutectic-forming Mn and peritectic-forming Mo leads to the formation of a substantial volume fraction of Al(MoMnFe)Si precipitates inside α-Al matrix, with a significant contribution to the high-temperature strengthening of Al–Si–Cu–Mg alloy. Shaha et al. [21] reported that the formation of both micro- and nano-sized Mo/Mn-rich dispersoids in inter- and intradendritic regions respectively enhanced high-temperature tensile properties of Al–Si–Cu–Mg alloys. Nevertheless, too high level of Mn also tended to increase the volume fraction of interdendritic compounds, thus deteriorating

the alloy mechanical properties [20]. Hence, we can infer that the introduction of appropriate types of transition metals and strict control of the addition levels is a critical step in generating a microstructure more favorable for high-temperature applications.

Moreover, there is no research in the literature with regard to the effects of adding Zr and V on high-temperature mechanical properties of secondary (recycled) Al–Si–Cu–Mg based alloys, one of the most used alloys for engine production, particularly for cylinder head castings [22]. The presence of trace (impurity) elements, such as Ti, Mn, Fe, Cr and Ni in minor levels in these alloys may induce changes in the solid-state precipitation sequence due to their possible interactions with deliberately-added transition metals, such as Zr and V, thus yielding the formation of various types of precipitates inside α-Al grains at higher volume fractions.

This study thus attempts to investigate the effect of adding Zr and V and age-hardening heat treatment on microstructural evolution and tensile properties of the secondary Al-7Si-3Cu-0.3Mg alloy, with the aim of forming a new type of thermally stable, intradendritic precipitates having potential in high-temperature strengthening of Al–Si based alloys.

2. Experimental procedure

A secondary Al-7Si-3Cu-0.3Mg alloy (EN AB-46300, equivalent to the US designation A320), supplied by Raffineria Metalli Capra as commercial ingots was used as a baseline material. Al-10Zr and Al-10V (in wt.%) waffle-shaped master alloys were used to add to the base alloy melt and prepare a new alloy. Hereafter, the new alloy prepared for this study is referred to as a (Zr/V-) modified alloy. The melting of ingots was conducted in an electrical-resistance furnace at 760 °C. To produce Zr/V-modified alloy, the pre-calculated amounts of Al-10Zr and Al-10V master alloys were added to the melt to achieve desired levels of Zr and V in the alloy. The H_2 gas level and the melt temperature were continuously monitored using an Alspek-H hydrogen gas analyzer machine and the melt was stirred and surface skimmed 15 min prior to pouring. The chemical composition was analyzed using optical spectroscopy on the specimens separately poured at the beginning and the end of every casting conditions; the averaged compositions of the base and Zr/V-modified alloys are listed in Table 1.

A steel mold was used to produce castings. The casting design can be seen in Ref. [23]. Boron nitride was used to coat the mold inner surfaces. At the time of pouring, the temperature of the die was increased to 250 °C. The temperature was monitored by means of thermocouples embedded in the die to ensure good reproducibility of the tests. The average secondary dendritic arm spacing *(SDAS)* of the produced castings was ∼15 μm in both the base and Zr/V-modified alloys.

Cylindrical tensile bars were sectioned from castings, and then analyzed using a Bosello SRE 80 industrial machine equipped with a macro-focus X-ray source to assure the soundness of the specimens.

The age-hardening heat treatment (T6 state) of some selected specimens was then performed in an air-circulating furnace; the solution heat treatment was performed at 485 °C for 24 h and then quenched in water at room temperature, followed by aging at 180 °C for 8 h. The temperature for solution heat treatment was selected on the basis of the results from differential scanning calorimetry (DSC) analyses performed in our previous research [24]. Longer solutionizing time was applied to enable the precipitation reactions involving transition metals, such as Zr and V, inside α-Al grains [25].

Several tensile specimens representing the base and Zr/V-modified alloys both in the as-cast and heat-treated states were chosen for microstructural analyses and sectioned from the cross-section of the gauge length. The specimens obtained were then mounted, ground and polished following the standard techniques. Optical microscopy (OM), scanning electron microscopy (SEM) equipped with energy-dispersive X-ray spectroscopy (EDS) and transmission electron microscopy (TEM) equipped with EDS were used to investigate the microstructure. Some microstructural features, such as the roundness of Si particles, and the fraction of Fe-rich compounds, were quantitatively analyzed using an image analyzer. Several optical micrographs, representing a total area of 5 mm^2, were captured from each specimen to obtain a statistical average of the analyzed parameters.

All the as-cast and heat-treated tensile bars were then machined to produce specimens with total length of 175 mm, a gauge length of 65 mm, and a diameter of 10 mm. The tensile tests were conducted on an MTS 810 tensile testing machine at a strain rate of 10^{-3} s^{-1}. The strain was measured using a 25-mm extensometer. The as-cast specimens were only tested at room temperature (20 °C), whereas the heat-treated specimens were tested at both room (20 °C) and high temperatures (200 and 300 °C). For the cases of high-temperature tests, the tensile specimens were held at testing temperature for 30 min before starting the test. At least four tensile tests were conducted for each condition. Experimental data were collected and processed to provide yield strength (*YS*), ultimate tensile strength (*UTS*) and elongation to fracture (*% El*).

3. Results

3.1. Microstructural evolution

Figure 1 shows typical as-cast microstructures observed in the base and Zr/V-modified alloys. The microstructure of the base alloy exhibits α-Al matrix, eutectic Si, $Al_{15}(FeMn)_3Si_2$ and Cu-rich phases (see Fig. 1a); in addi-

Table 1. The chemical composition of the base and Zr/V-modified alloys (wt.%).

Alloy type	Si	Fe	Cu	Mn	Mg	Zn	Cr	Ni	Ti	Pb	V	Zr	Al
Base	7.8	0.46	3.1	0.23	0.32	0.78	0.040	0.030	0.1	0.03	0.01	0.01	bal.
Modified	7.5	0.45	3.0	0.22	0.30	0.76	0.037	0.025	0.1	0.03	0.30	0.15	bal.

tion, small and rare $Al_8Mg_3FeSi_6$ and Ca-, Bi-, Pb-rich particles are observed in the microstructure, as discussed in detail in our previous study [26, 27]. Microstructural characterization of the Zr/V-modified alloy (see Fig. 1b) revealed the presence of Zr-rich compounds in addition to the phases observed in the base alloy; these Zr-rich intermetallic compounds are identified as $(AlSi)_3(ZrTi)$ phase [24]. The $(AlSi)_3(ZrTi)$ compounds reside in the interdendritic regions in a size range of 10 µm (Fig. 1). The excess solute of V rejected into the interdendritic liquid during alloy solidification was found to be solely bound to pro-eutectic α-$Al_{15}(FeMn)_3Si_2$ compounds (see Fig. 2), thus slightly increasing the fraction of Fe-rich phases from 0.4 % in the base alloy to 0.5 % in the Zr/V-modified alloy. In our previous study [24], a small amount of pro-eutectic $(AlSi)_2 \cdot (VTiMn)$ compounds were detected in the microstructure generated at a lower cooling rate corresponding to the *SDAS* value of ∼65 µm. In the present study, however, the higher cooling rate corresponding to an *SDAS* of ∼15 µm seems to retain more V in the α-Al solid solution, thus avoiding the precipitation of pro-eutectic $(AlSi)_2(VMn)$ phase.

As shown in Fig. 3, both V and Zr added into the alloy tended to mainly concentrate in the α-Al grain interiors.

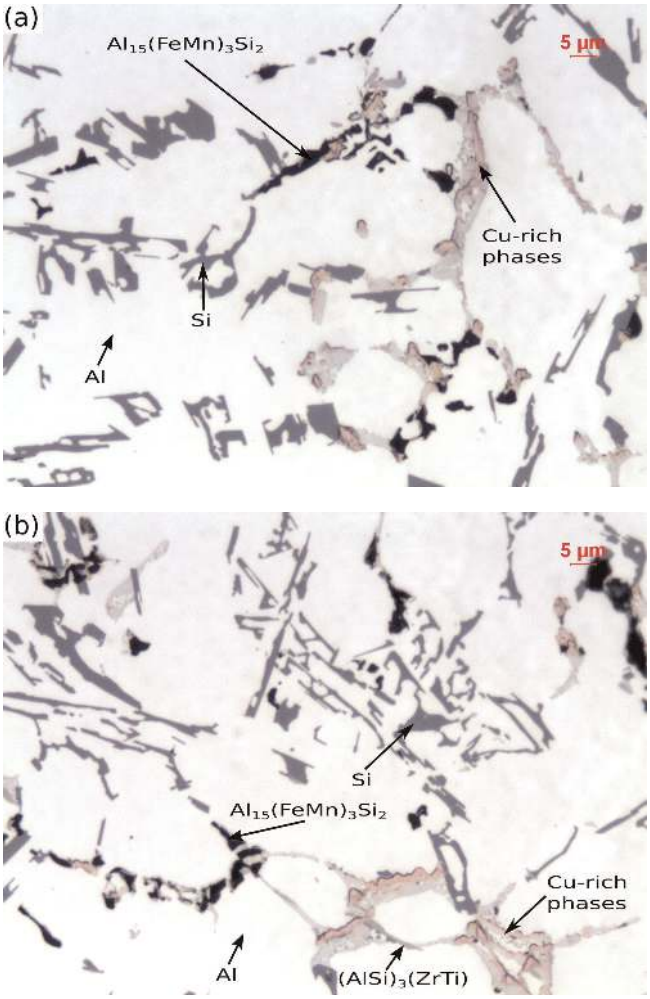

Fig. 1. Typical microstructures of the (a) base, and (b) Zr/V-modified alloys in as-cast states. The samples were etched in a mixture of H_2O and H_2SO_4, preheated to 70 °C to highlight Fe-rich compounds.

Figure 3 also shows how the peritectic-forming Zr and Ti tended to segregate towards the core/centre of α-Al grains due to their partitioning coefficient, which is larger than unity, while Mn showed more homogeneous distribution over the cross-section of α-Al matrix as its partitioning coefficient is equal to unity. In other words, non-equilibrium solidification can result in the inhomogeneous distribution of Zr and V inside the α-Al grains, i. e. positive and negative segregation of these elements in dendrite cores and edges, respectively, due to limited solid-state diffusion (see Fig. 3).

Figure 4 shows the typical microstructures representing the base and Zr/V-modified alloys after T6 heat treatment. Qualitative comparison of as-cast and T6 heat-treated microstructures indicates how applying heat treatment changed the size and morphology of eutectic Si particles and led to the dissolution of Cu/Mg-rich interdendritic particles into the α-Al matrix. It is known that eutectic Si particles tend to undergo fragmentation and spheroidization during solution heat treatment [28]. Quantitative analysis of eutectic Si particles in the base and Zr/V-modified alloys revealed that the roundness value changes from ∼5 in the as-cast state to ∼2 in the heat-treated state. Only small amounts of Cu-rich compounds still exist in interdendritic regions (see Fig. 4) indicating their incomplete dissolution into the α-Al matrix, whereas the α-$Al_{15}(FeMn)_3Si_2$ and $(AlSi)_3(ZrTi)$ phases showed no tendency to dissolve into the α-Al matrix and remained stable in grain boundaries and interdendritic regions (Fig. 4 and Fig. 5).

X-ray mapping analyses (Fig. 5 and Fig. 6) suggest that the undissolved Cu-rich particles are mainly $Al_5Si_6Cu_2Mg_8$ and some blocky Al_2Cu compounds, which are typically observed in Al–Si–Cu–Mg alloys; this indicates the necessity for higher solutionizing temperature. Moreover, the trace amounts of Ni (∼250 ppm) appear to be sufficient to form some thermally more stable Al-Ni-Cu interdendritic intermetallics, which remained undissolved into the α-Al matrix during the solutionizing stage (Fig. 6).

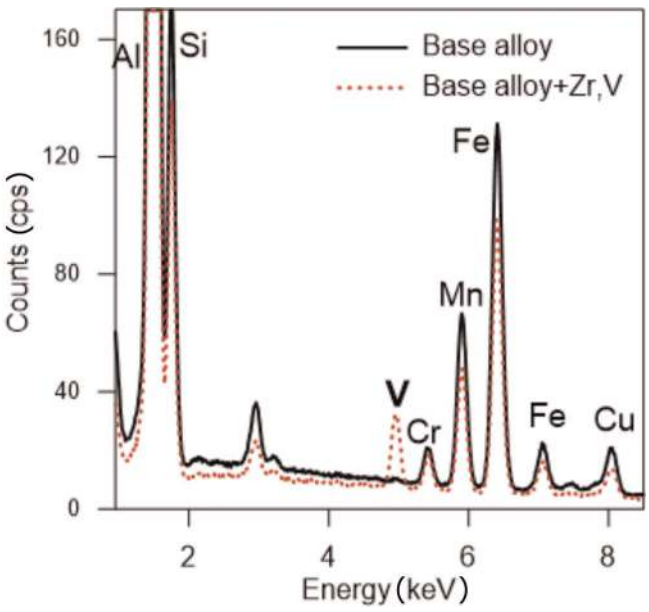

Fig. 2. Typical EDS spectra of α-$Al_{15}(FeMn)_3Si_2$ phase observed in the (a) base, and (b) Zr/V-modified alloys in as-cast states.

It is known that the mechanical properties of Al–Si alloys containing Cu and Mg can be significantly improved by applying the age-hardening heat treatment. The bright field (BF) TEM micrographs in Fig. 7 show that precipitation occurred upon T6 heat treatment in the intradendritic regions (α-Al grain interiors). The needle-like precipitates, which are believed to be θ′ phase [29], are dominant throughout the microstructure (Fig. 7). Detailed characterization of the solid-state precipitation reactions involving Cu and Mg in Al–Si–Cu–Mg alloys can be found elsewhere [29–31]. Comparison of the microstructures of the base and Zr/V-modified alloys revealed the presence of Zr/V-rich precipitates inside the α-Al matrix of Zr/V-modified alloy. Due to limited diffusivity of Zr and V in α-Al matrix, the solid-state precipitation reactions involving these elements require higher temperatures than that applied during the aging stage. Microstructural investigations of the alloys after solution heat treatment and quenching stages confirmed the occurrence of solid-state precipitation reactions involving Zr and V during solution heat treatment, as shown in Fig. 8. It is evident that the density of precipitates in the Zr/V-modified alloy is substantially higher than that of the base alloy.

The EDS analysis of the base alloy (Fig. 9) suggests that a few precipitates observed in the α-Al grain interiors are of α-Al(MnFe)Si type [32, 33]. The EDS investigation of the precipitates formed in the Zr/V-modified alloy suggests the presence of three different types of Zr- and V-rich phases (Fig. 10). The precipitate numbered 1 in Fig. 10a is believed to be the α-Al(MnVFe)Si phase, which is also observed in the grain interiors of the base alloy in the form of α-Al(MnFe)Si [33–35]. The α-Al(MnVFe)Si particles appear in plate-like morphology with an average size of 100 nm and account for a major part of the precipitates formed during solution heat treatment of the Zr/V-modified alloy. The role of V appears to be significant in promoting the precipitation of α-Al(MnFe)Si by substituting Mn in

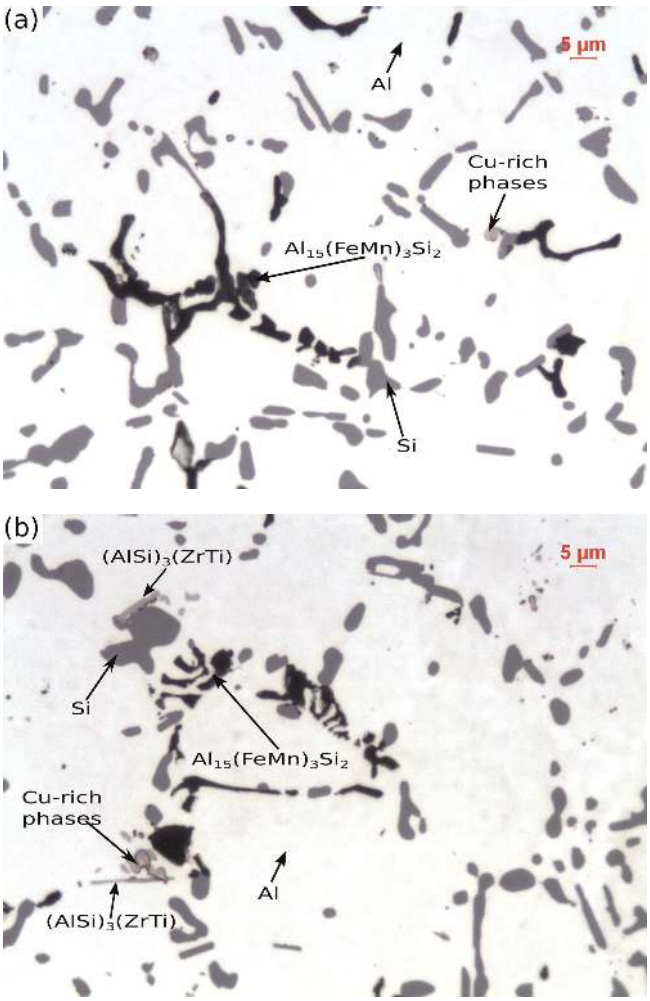

Fig. 4. Typical microstructures of the (a) base, and (b) Zr/V-modified alloys in the heat-treated states. The samples were etched in a mixture of H_2O and H_2SO_4, preheated to 70 °C to highlight Fe-rich compounds.

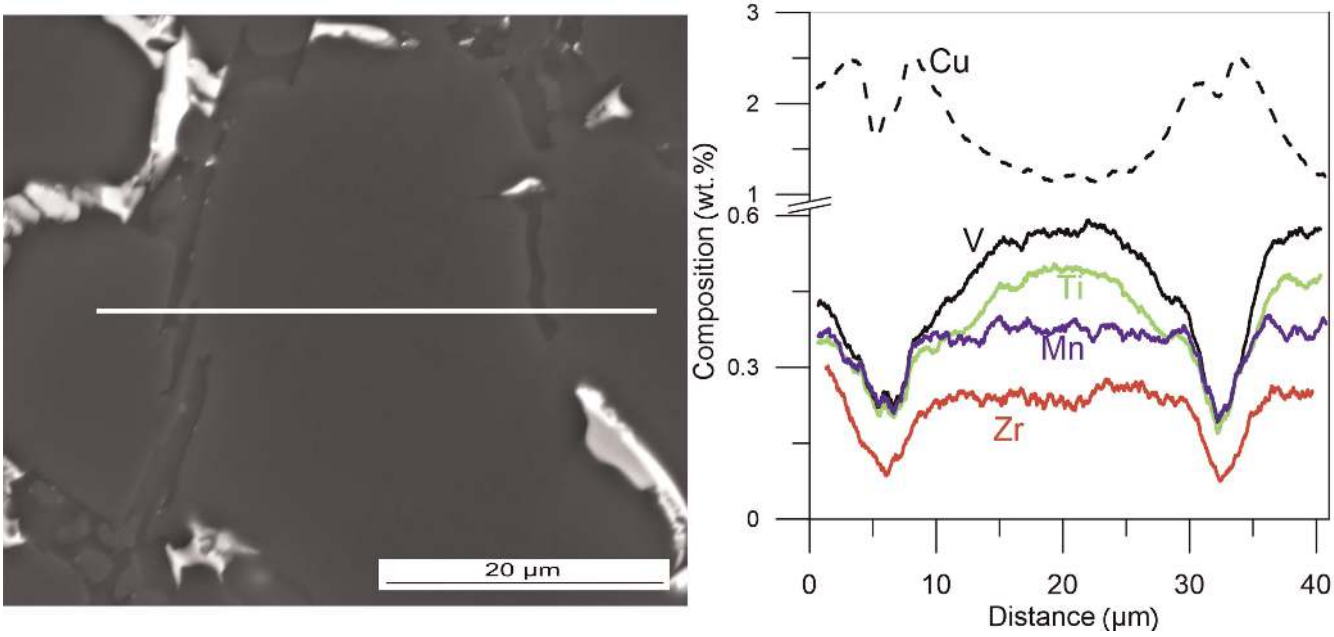

Fig. 3. SEM image of α-Al grain in Zr/V-modified alloy with corresponding EDS line-scan, showing the distributions of Zr, V, Ti, Mn and Cu elements.

this phase. The flaky-like Zr-rich precipitates numbered 2 in Fig. 10a and identified as $(AlSi)_3(ZrTi)$ in Ref. [19] are rarely observable in the α-Al grain interiors, which can be due to the low solubility of both Zr and Ti in α-Al. The irregular-shaped V-rich precipitate numbered 3 in Fig. 10a is believed to be an $(AlSi)_2(VCr)$ phase according to its composition; however, further TEM investigations seem necessary to conduct full crystallographic studies of this phase. This precipitate is also hardly apparent in the microstructure (grain interiors), which can be explained by more preferential involvement of V in the precipitation of α-Al(MnVFe)Si phase.

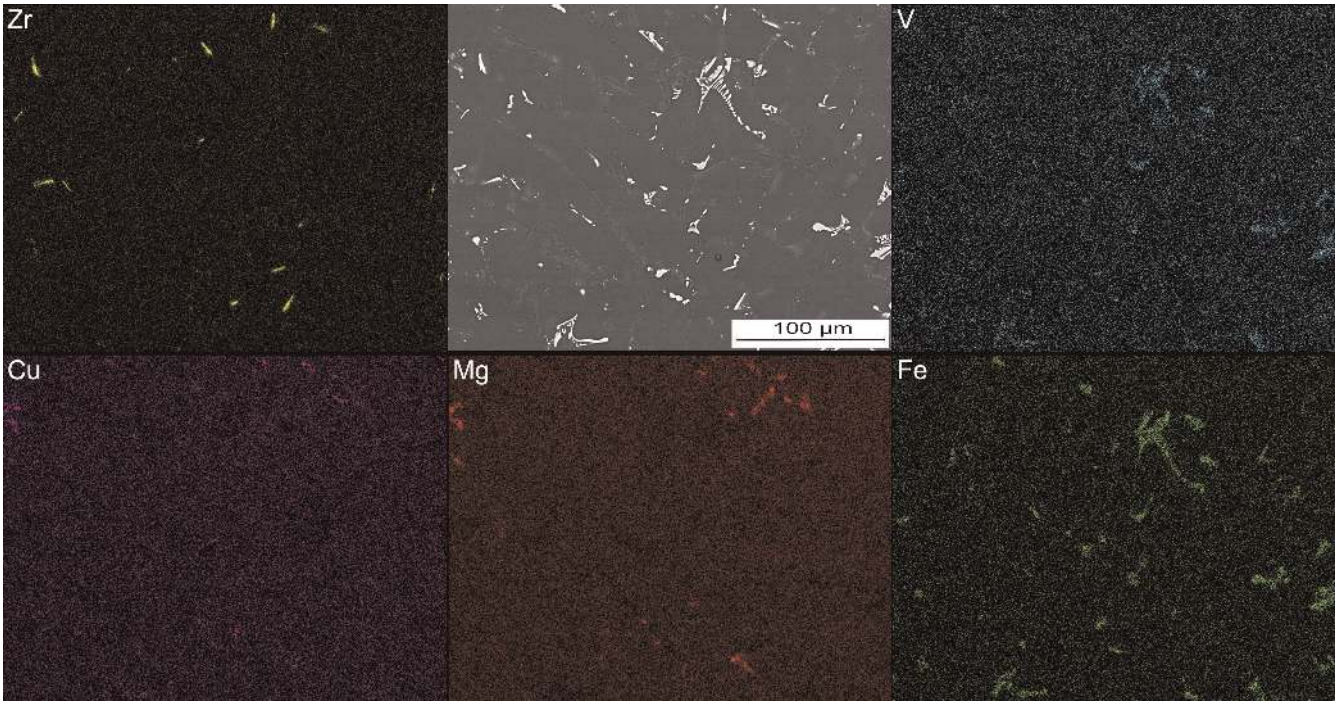

Fig. 5. Backscattered electron image of a typical microstructure of Zr/V-modified alloy after T6 heat treatment with corresponding EDS composition maps, showing the distributions of Zr, V, Cu, Mg and Fe elements.

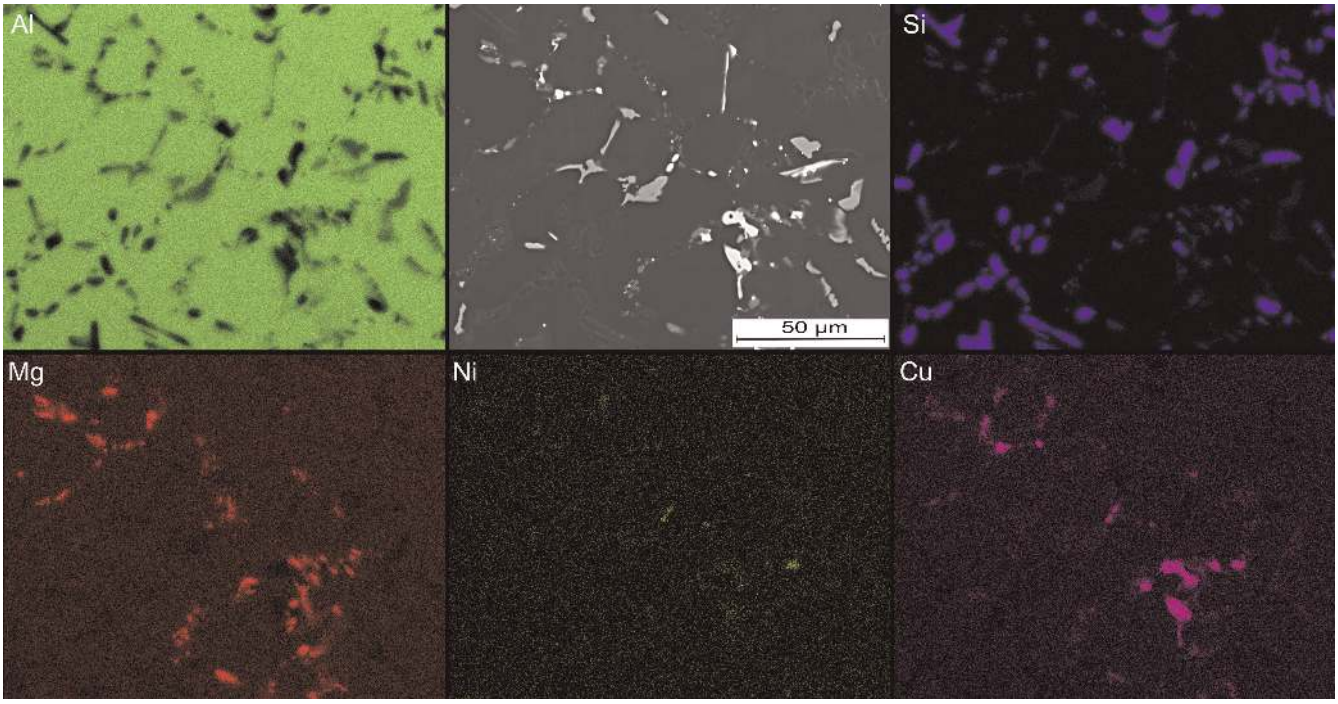

Fig. 6. Backscattered electron image of a typical microstructure of Zr/V-modified alloy after T6 heat treatment with corresponding EDS composition maps, showing the distributions of Al, Si, Mg, Ni and Cu elements.

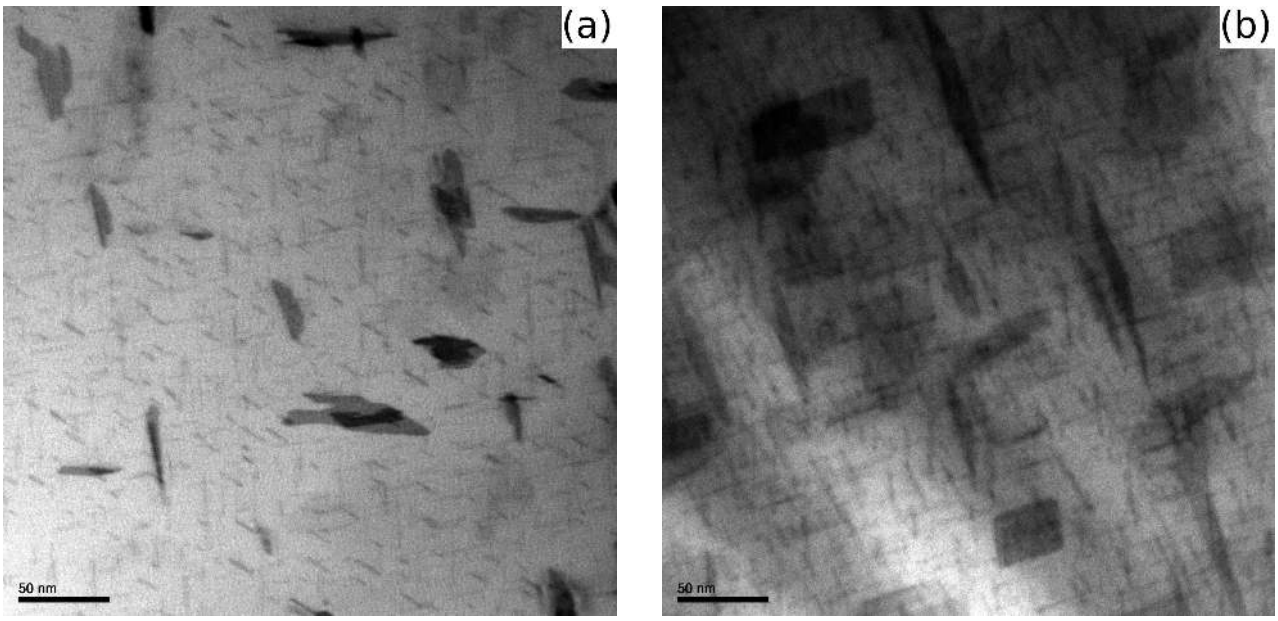

Fig. 7. BF TEM micrographs showing the precipitation observed after T6 heat treatment in the (a) base, and (b) Zr/V-modified alloys.

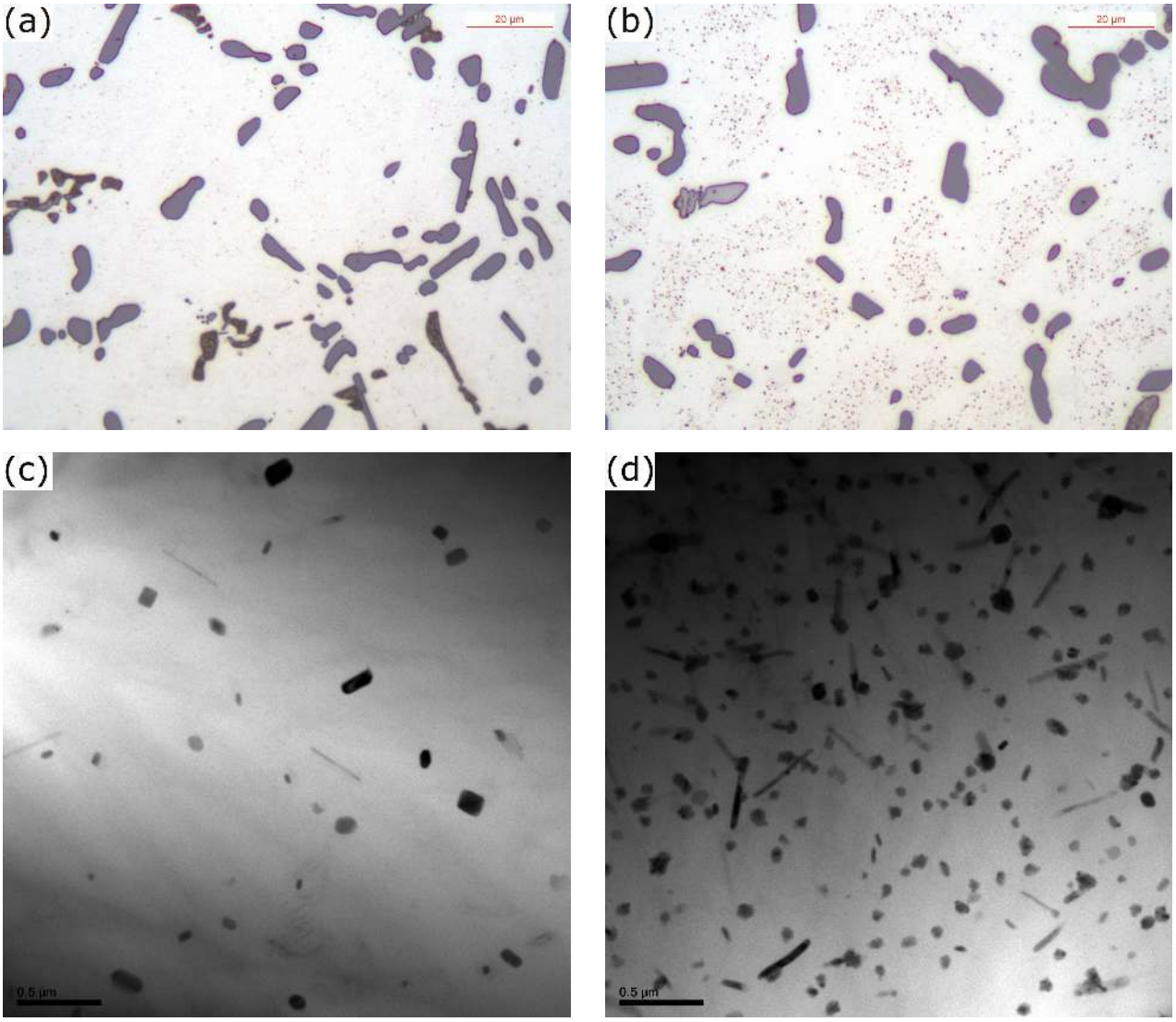

Fig. 8. (a,b) Optical micrographs, and (c,d) BF TEM micrographs showing the precipitates formed during solution heat treatment of the (a,c) base, and (b,d) Zr/V-modified alloys. Optical micrographs were obtained from samples etched in 1 % HF for 30 s to reveal secondary precipitates.

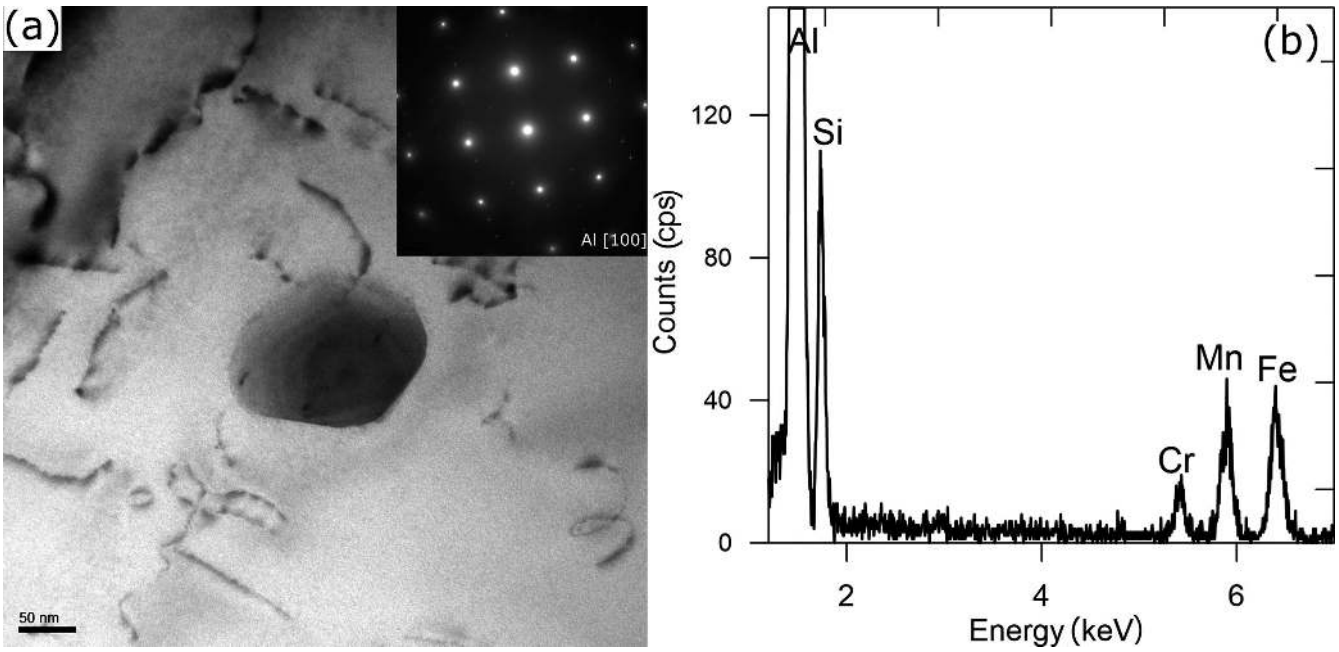

Fig. 9. (a) BF TEM micrograph showing the α-Al(MnFe)Si precipitate formed in α-Al grain interior during solution heat treatment of the base alloy, and (b) EDS spectrum of α-Al(MnFe)Si precipitate shown in Fig. 9a.

3.2. Tensile properties

Table 2 presents the room-temperature tensile properties in the as-cast and heat-treated states of both the base and Zr/V-modified alloys. The response of both the base and Zr/V-modified alloys to heat treatment seems to be similar. While the yield strength (*YS*) and ultimate tensile strength (*UTS*) of the base alloy increased from 155 and 248 MPa in the as-cast state to 364 and 415 MPa in T6 heat treated states, respectively, the elongation to failure (*% El*) remained almost constant in the range of ∼2 % in both the as-cast and heat-treated states. The Zr/V-modified alloy exhibits slightly better YS in both the as-cast and heat-treated states (see Table 2).

Figure 11 shows the tensile properties of the base and Zr/V-modified alloys after T6 heat treatment as a function of testing temperature. It is evident that tensile properties tend to decrease as the testing temperature increases [36]; the *YS* and *UTS* of the base alloy decreased from approximately 364 and 415 MPa at room temperature to about 262 and 271 MPa at 200 °C, followed by a further decrease to 83 and 86 MPa at 300 °C testing temperatures respectively, whereas the *% El* increased from ∼2 % at 20 °C to approximately 2.5 % at 200 °C, and 8 % at 300 °C. Adding Zr and V showed no significant improvement on room-temperature tensile properties of the alloy. However, with increasing the testing temperature, the positive effects of Zr and V became more evident (Fig. 11a and c). The *UTS* and *YS* of Zr/V-modified alloys at 300 °C testing temperature are higher by around 20 % compared to the base alloy. The improvement, however, was also followed by a slight decrease in *% El* (Fig. 11c).

3.3. Fractographic observations

Typical examples of SEM fractographs observed on the fractured surfaces of the studied alloys tested at 20 and 300 °C temperatures are shown in Fig. 12. The presence of casting defects, such as oxide inclusions and shrinkage, appear to govern the fracture of the tensile-tested specimens; these casting defects can act as preferential sites for crack initiation [37]. Once the damage is initiated by the casting defects, the propagation occurs through the cracking of interdendritic brittle phases, such as eutectic Si and Fe/Cu-rich intermetallic particles (see Fig. 13 and Fig. 14), due to the development of internal stresses in the particles by plastic deformation. Microcracks originating in those interdendritic, brittle intermetallics propagate through the α-Al matrix and subsequently connect to each other to produce the main crack.

As can be seen in Fig. 13, the main fracture profile line of the base and Zr/V-modified alloys in the as-cast state reflects the shape of the dendritic structure. The cleavage fracture of eutectic Si and Cu/Fe-rich intermetallics is evident. The plastically deformed microregions (micronecks) of the α-Al dendrites are also noticed in both the base and Zr/V-modified alloys, which suggests that a mixed intergranular-transgranular fracture mode was operative in the as-cast state of the studied alloys, with the intergranular brittle fracture mode being the dominant one. The SEM fractograph representing Zr/V-modified alloy in the as-cast state also shows the tear ridges and fractured brittle phases, such as Si and Cu/Fe-rich intermetallics (Fig. 15a). Since the α-Al matrix is relatively soft and ductile, the stress incompatibilities evolved at the particle/matrix interfaces favour cracking of brittle, interdendritic phases, which dominates the fracture mode [38].

Applying T6 heat treatment showed no significant influence on the fracture profile of the alloys tested at room temperature (see Fig. 14a and d and Fig. 15b). Although the solutionizing stage caused spheroidization of eutectic Si particles, some Si particles still remained elongated and coarser and these particles crack more easily as they possess lower fracture stress [39–41]. Although more spheroi-

dized Si particles in heat-treated alloys would contribute to higher elongation to failure, the hardening of α-Al matrix induced by T6 heat treatment restrains the plastic deformation of the α-Al matrix. These microstructural changes can be responsible for having nearly the same elongation to failure observed in both the as-cast and heat-treated states of the studied alloys.

When the testing temperature was increased to 200 °C, the fracture profile of the studied alloys remained almost unchanged compared to the alloys tested at room tempera-

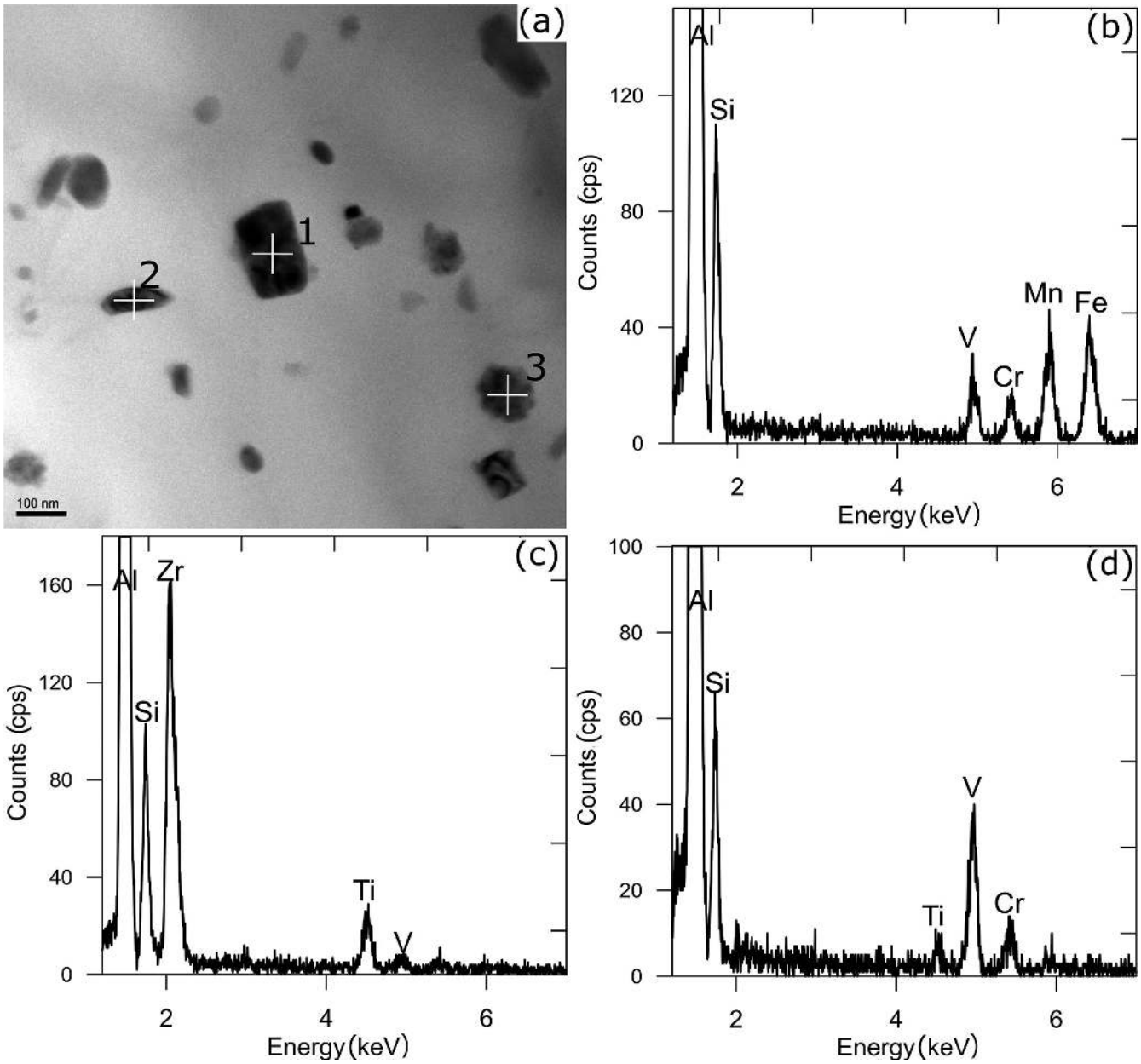

Fig. 10. (a) BF TEM micrograph showing the precipitates formed in α-Al grain interiors during solution heat treatment of Zr/V-modified alloy; (b) EDS spectrum of Al(MnVFe)Si precipitate numbered 1 in Fig. 10a; (c) EDS spectrum of $(AlSi)_3(ZrTi)$ precipitate numbered 2 in Fig. 10a; (d) EDS spectrum of $(AlSi)_2(VCr)$ precipitate numbered 3 in Fig. 10a.

Table 2. Tensile properties with corresponding standard deviation (in parentheses) of the base and Zr/V-modified alloys before and after T6 heat treatment at room temperature.

Alloy type	As-cast			T6 treatment		
	YS (MPa)	*UTS* (MPa)	*% El*	*YS* (MPa)	*UTS* (MPa)	*% El*
base	155 (5.2)	248.2 (2.8)	1.95 (0.20)	364.4 (2.8)	415.17 (4.6)	1.98 (0.26)
modified	158.6 (0.3)	248.8 (1.5)	1.77 (0.12)	368.8 (2.1)	414.8 (3.5)	1.7 (0.30)

ture, even though some dimples can be seen at fracture surfaces; a slight increase in the elongation to failure of the alloys tested at 200 °C compared to the alloys tested at room temperature also confirms the occurrence of slight plastic deformation. The absence of significant amount of dimples on the fracture surfaces of the alloys tested at 20 and 200 °C (Fig. 15a–c) is an indication of the brittle fracture mode that was operative in these investigation conditions.

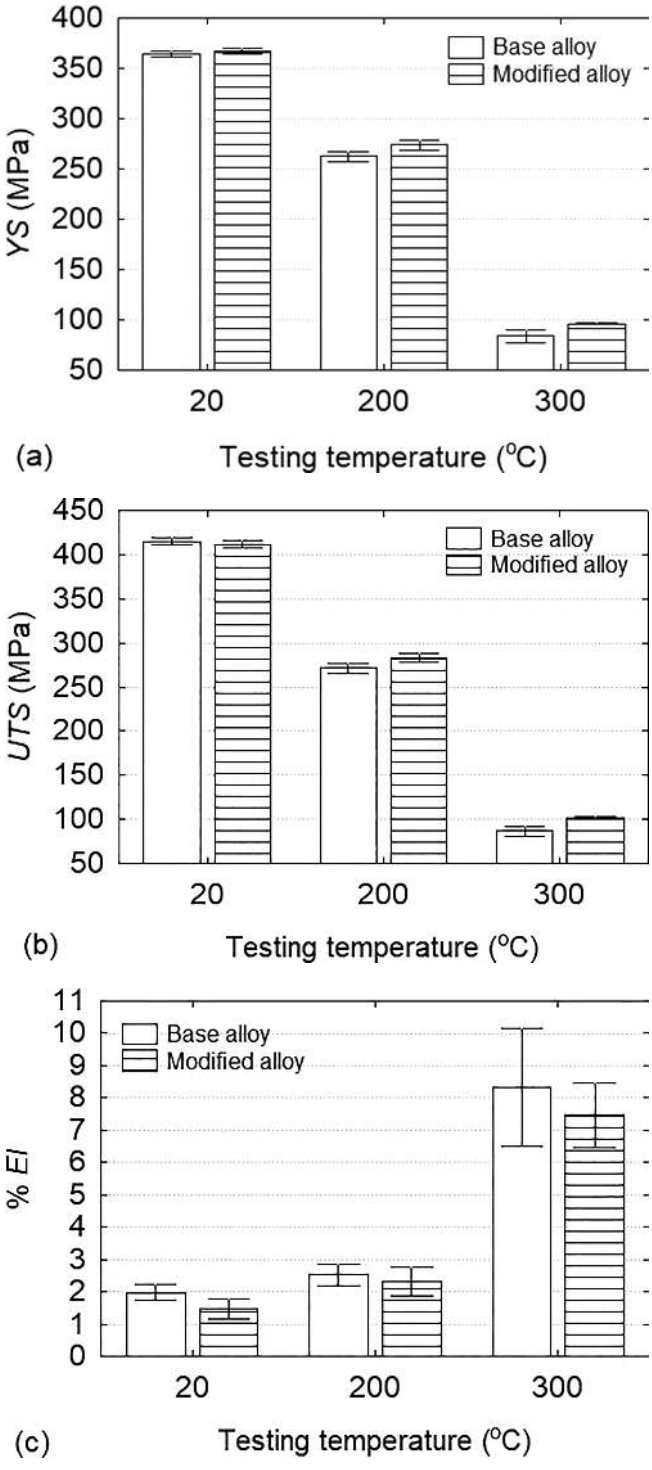

Fig. 11. A comparison of the tensile properties of the base and Zr/V-modified alloys after T6 heat treatment, obtained at different testing temperatures: (a) yield strength, (b) ultimate tensile strength, and (c) elongation to failure.

Further increase of the testing temperature to 300 °C resulted in brittle-to-ductile transition of fracture mode in both alloys (see Fig. 12). Although interdendritic particle cracking and micronecks can be also seen on the fractured surfaces (see Fig. 14c and f), the fracture path mainly follows the sheared α-Al matrix (see Fig. 12). Fracture of the alloys tested at 300 °C was dominated by ductile dimple fracture with the cavities containing multiple fragmented intermetallic phases (Fig. 15d) [38, 42]. Note that at low temperatures, a single dominant cleavage crack of brittle, interdendritic phases was observable on the fracture surfaces (Fig. 15a–c). When the testing temperature is raised to 300 °C, the α-Al matrix becomes much softer than at room temperature, thus increasing the plasticity of the alloys. At high temperatures, the α-Al matrix is more prone to deformation, which implies that internal stresses originated by the structural inhomogeneity can be partially recovered at the expense of the matrix.

4. Discussion

4.1. Microstructural evolution and phase transformations

Although the added level of Zr in this study is quite low (0.15 %), a limited amount of primary $(AlSi)_3(ZrTi)$ compounds with flaky morphology can be seen throughout the microstructure (Fig. 1b and Fig. 5). The majority of Zr and V added to the alloy tends to reside inside α-Al matrix (Fig. 3) and contribute to the refinement of the α-Al grains [24]. The amount of V rejected to interdendritic regions was solely bound to pro-eutectic α-$Al_{15}(MnFe)_3Si_2$ phase (Fig. 1 and Fig. 5), which caused a slight increase of the fraction of interdendritic α-$Al_{15}(MnFe)_3Si_2$ in the microstructure. The previous investigation [24] revealed the presence of interdendritic $(AlSi)_2(VMn)$ phase in the slowly-solidified microstructure. In contrast, in the present study, the higher cooling rate appears to facilitate the α-Al solid solution to retain more V during solidification and, as a result, a lower amount of V can segregate to interdendritic regions, thus suppressing the formation of $(AlSi)_2(VMn)$ phase. It is worthy noting that the addition levels of V (0.3 wt.%) and Zr (0.15 wt.%) selected in the present study, showed no significant influence on the fraction of insoluble intermetallics.

Solution treatment, which is the first stage of T6 heat treatment, is normally applied to dissolve interdendritic Cu- and Mg-rich particles into the α-Al matrix, and also spheroidize the eutectic silicon particles [3, 28, 43]; however, this study also revealed that the solutionizing stage can also promote the precipitation of a large volume fraction of Zr/V-rich precipitates inside α-Al matrix (see Fig. 8b and d). Considering that the peritectic-forming Zr and V elements tend to partition towards the α-Al grain cores during solidification and remain in α-Al solid solution (Fig. 3) and their excess amounts tended to form the insoluble, interdendritic intermetallics (see Fig. 5), it can be thus inferred that the supersaturated Zr and V amounts in solid solution obtained during non-equilibrium solidification can only be involved in the solid-state precipitation occurring inside α-Al matrix.

As mentioned earlier, a very limited amount of α-Al(MnFe)Si precipitates formed in α-Al grain interiors of the base alloy at the solution heat treatment stage (see

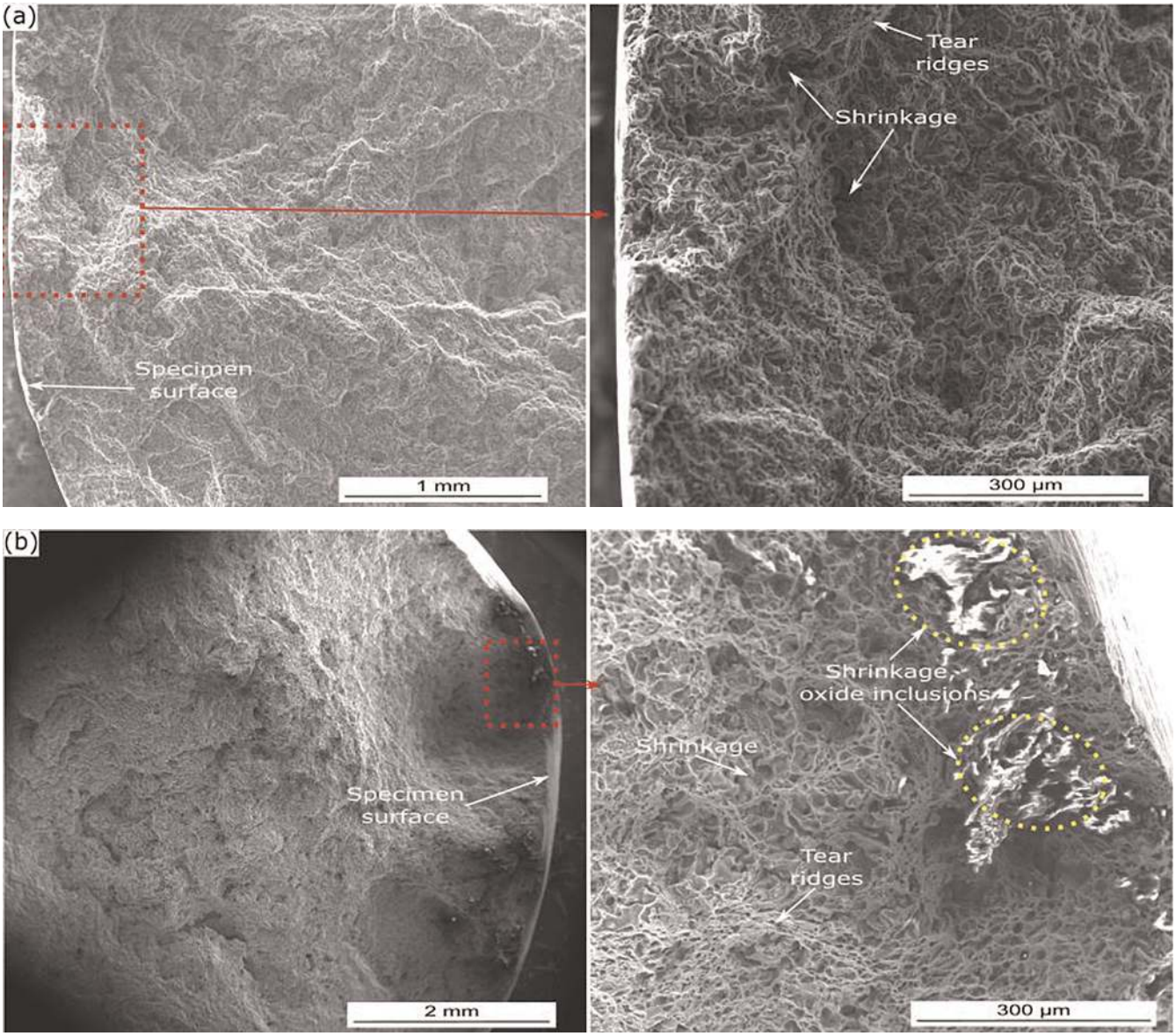

Fig. 12. Secondary electron micrographs showing the fracture surfaces of Zr/V-modified Al-7Si-3Cu-0.3Mg alloy in T6 heat-treated state and tested at (a) 20, and (b) 300 °C temperatures. The location of crack initiation, and the casting defects, such as shrinkage and oxide inclusions, that initiated the crack can be seen.

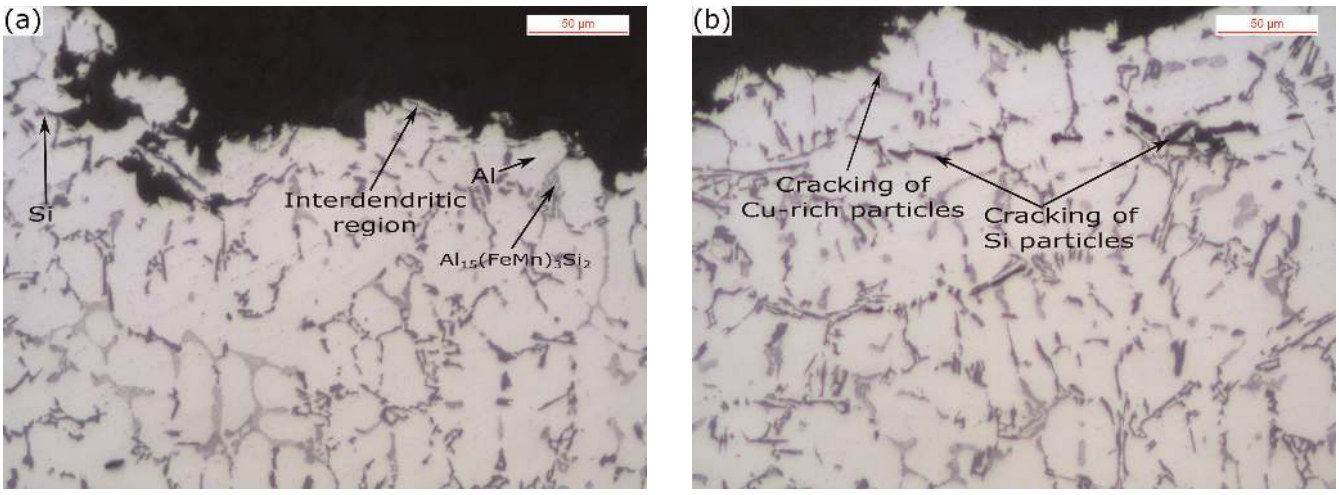

Fig. 13. Optical micrographs of fracture profiles, showing a mixed transdendritic–interdendritic fracture on the (a) base, and (b) Zr/V-modified alloys.

Fig. 8a and c). Since Mn is normally added to promote the formation of α-$Al_{15}(MnFe)_3Si_2$ over β-Al_5FeSi during solidification [27], some amount of Mn can also accumulate into primary α-Al matrix during solidification. Non-equilibrium solidification, in turn, can also result in the supersaturation of Mn, Cr and Fe in α-Al solid solution; hence, the solid-state precipitation reaction involving Mn occurred during solution heat treatment.

As stated earlier (Section 3.1), the presence of V in the Zr/V-modified alloy significantly increased the density of α-Al(MnFe)Si intradendritic precipitates. This behavior can be explained by the peritectic nature of V and its ability to substitute Mn in α-Al(MnFe)Si phase. The combined involvement of V and Mn to form precipitates in the α-Al grain interiors is highly beneficial; the partitioning behavior of V during solidification is opposite to that of Mn and this behavior can lead to a more uniform distribution of the precipitates. Moreover, both Mn and V are the slow diffusers, with relatively high solid solubility in α-Al; hence, the solid-state precipitation of α-Al(MnVFe)Si phase occurs in relatively high-volume fractions. It can also be noted that the size of precipitates is in the order of 100 nm (see Fig. 9 and Fig. 10), which is significantly larger than the Cu-rich precipitates formed at aging heat treatment stage (see Fig. 7). Muggerud et al. [32] investigated the solid-state precipitation behavior of α-Al(MnFe)Si in direct-chill cast 3xxx alloy annealed at 375 °C for various times, and it has been found that too long annealing time considerably decreases the volume fraction of precipitates due to their coarsening behavior. Optimization of solution heat treatment parameters of secondary Al-7Si-3Cu-0.3Mg alloy with Zr and V additions may result in the precipitation of α-Al(MnVFe)Si in smaller sizes and higher number density, thus contributing much better to the high-temperature strengthening of Al–Si alloys. The majority of α-Al(MnVFe)Si precipitates possess a nearly cubic shape and seem to have the same orientation to the α-Al matrix. The α-Al(MnFe)Si dispersoids have recently been shown to be partly coherent with the Al matrix [37].

The solutionizing stage also caused the α-Al solid solution supersaturated with Zr to decompose and precipitate inside the α-Al matrix in the form of $(AlSi)_3(ZrTi)$ phase in a very limited amounts and average length of around 100 nm. Gao et al. [21] have reported how Ti and V can accumulate in Al_3Zr phase [44]; however, in the present study, only Ti, which is present in the alloy as a trace element, tended to substitute Zr, whereas V showed no tendency to contribute to the formation of $(AlSi)_3(ZrTi)$ phase. This could be due to a more favorable involvement of V in the formation of α-Al(MnVFe)Si phase. Sepehrband et al. [25] revealed that solution heat treatment of A319 alloy containing Zr, at 505 °C for 24 h caused the precipitation of Al_3Zr particles with a length of around 210–250 nm in grain interiors. The smaller size of these rod-like precipitates observed in the present study could be due to the lower solutionizing temperature (485 °C) applied. In a recent study, the $(AlSi)_3(ZrTi)$ precipitates have been shown to be partly coherent with the Al matrix [19].

Small amounts of V also appear to be bound to irregular-shaped V-rich precipitate, which is believed to be $(AlSi)_2 \cdot (VCr)$ phase, in the α-Al grain interiors, however, further crystallographic investigations of this precipitate are necessary.

It is worth noting that the presence of several types of transition metals, such as trace (impurity) Mn, Fe, Ti and Cr, and deliberately-added Zr and V, in the Zr/V-modified alloy yielded the formation of a substantial volume fraction of Zr/V-rich precipitates during solution heat treatment stage (see Fig. 8).

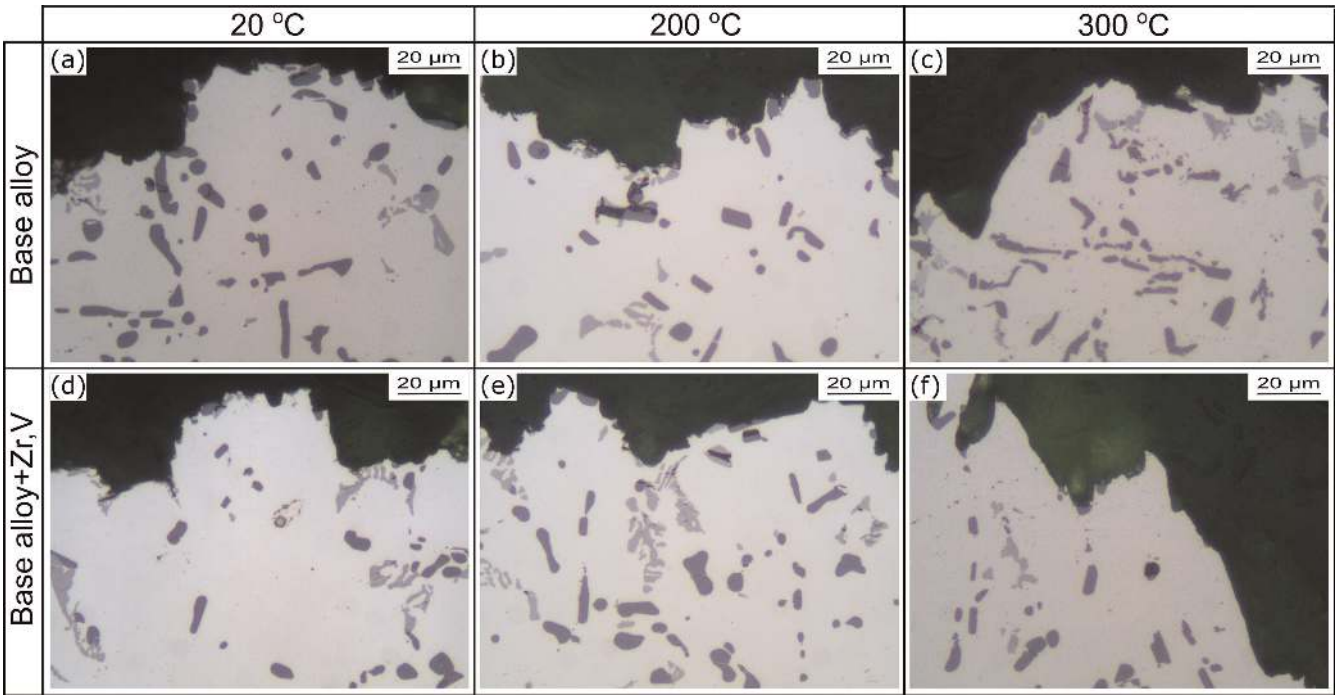

Fig. 14. Optical micrographs of the tensile fracture profile of the (a,b,c) base, and (d,e,f) Zr/V-modified alloys tested at (a,d) 20, (b,e) 200, and (c,f) 300 °C temperatures.

4.2. Microstructure–property relationship

The addition of Zr and V showed a slight influence on the tensile properties of Zr/V-modified alloy in the as-cast state; the *YS* increased slightly by ~5 MPa, which could be associated with the contribution of alloying additions to solid solution strengthening [45].

The role of T6 heat treatment in the strengthening of Al–Si–Cu–Mg based alloys is well-known [28]. The solid-state precipitation reactions involving Cu and Mg can provide significant strengthening by precipitation hardening [28]; comparison of the tensile properties of the base and Zr/V-modified alloys reveals slightly higher *YS* by ~4 MPa in Zr/V-modified alloy. This indicates that the enhanced properties of both alloys upon T6 heat treatment are primarily the consequence of intradendritic Cu/Mg-rich precipitates while the influence of intradendritic Zr/V-rich particles on alloy strength at room temperature appears to be negligible.

Increasing the testing temperature decreased the tensile properties (*UTS* and *YS*) of both alloys (Fig. 11a and b). It was also noticed (Fig. 11a and b) that *UTS* is more sensitive to temperature compared to *YS* of the alloys [46]. With increasing the temperature, the cross slips are thermally activated by climbing of dislocations resulting in the reduction of material strength [13, 21, 36, 47]. In addition, the solute diffusion of Cu and Mg becomes increasingly effective in promoting precipitate coarsening within the matrix, hence further contributing to the alloy softening [5, 36]. Comparison of the tensile properties of the alloys as a function of testing temperature (Fig. 11a and b) indicates that the effect of Zr and V additions seems to be more evident at high temperatures; both the *YS* and *UTS* parameters of the Zr/V-modified alloy are higher by ~20 % with respect to the base alloy. This improvement is attributed to the formation of intradendritic V/Zr-rich precipitates, which are much more thermally stable in comparison with the Cu/Mg-rich precipitates.

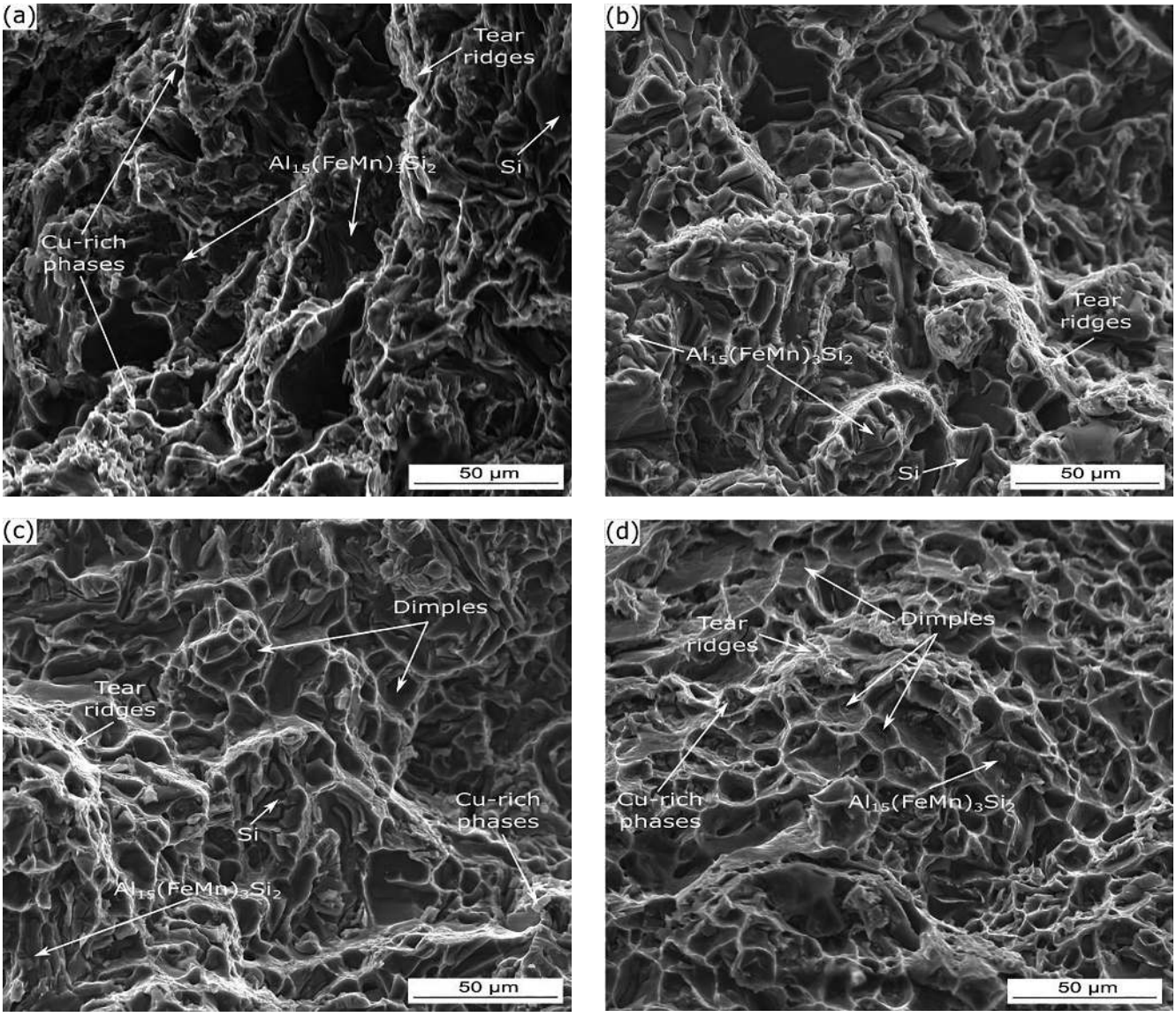

Fig. 15. Secondary electron micrographs of fractured surfaces of Zr/V-added Al-7Si-3Cu-0.3Mg alloy in (a) as-cast, and (b,c,d) T6 heat-treated states and tested at (a,b) 20, (c) 200, and (d) 300 °C temperatures.

The effect of adding Zr and V on elongation to failure remains almost negligible (see Fig. 11c), which can be explained by the fact that both Zr and V tended to concentrate mainly in grain interiors during solidification, and showed less impact on the evolution of insoluble, interdendritic intermetallics.

5. Conclusions

The effects of combined V and Zr additions, and heat treatment on the microstructure and mechanical properties of the secondary Al-7Si-3Cu-0.3Mg alloy were investigated. The following conclusions can be drawn from this study.

The majority of Zr and V added to the alloy was retarded inside α-Al matrix during solidification. The excess Zr amount that was rejected to interdendritic regions during alloy solidification was involved in the formation of flaky-like, interdendritic $(AlSi)_3(ZrTi)$ compounds, whereas excess V was bound to script-like $Al_{15}(MnFe)_3Si_2$ phase. A slight increase in yield strength of Zr/V-modified alloy in the as-cast state can be attributed to the solid solution hardening effects of V and Zr.

Upon heat treatment, the interdendritic intermetallics containing Zr and V, such as $(AlSi)_3(ZrTi)$ and $Al_{15}(FeMnV)_3Si_2$ compounds, remained undissolved in the α-Al matrix. The supersaturated solid solution of Zr and V in α-Al matrix, obtained during solidification, tended to decompose and precipitate inside α-Al grains during the solution heat treatment stage. The interaction between the deliberately-added Zr and V, and impurity (trace) Mn, Fe, Ti and Cr elements promoted the formation of a substantial volume fraction of multiple intradendritic, nano-sized precipitates: the blocky-like α-Al(MnVFe)Si, the flaky-like $(AlSi)_3(ZrTi)$ and the irregular-shaped $(AlSi)_2(VCr)$ phases. The α-Al(MnVFe)Si accounted for the major part of the thermally stable phases formed during the solutionizing stage; the interaction between peritectic-forming V and eutectic-forming Mn to form the α-Al(MnVFe)Si precipitate is believed to be highly beneficial due to their opposite partitioning behavior, as well as their higher solubility and lower diffusivity in α-Al matrix. Increase in the *UTS* and *YS* of Zr/V-modified alloy with respect to the base alloy at elevated temperatures are believed to be the consequence of the thermally stable precipitates formed during solution heat treatment.

This work was developed at University of Padova within the ERASMUS MUNDUS Project (Silkroute – Strand 1/Lot L09, project n. 545765). The author would like to acknowledge Raffineria Metalli Capra Spa (Brescia, Italy) for the experimental support to the research.

References

[1] Y. Birol: Mater. Sci. Technol. 28 (2012) 363. DOI:10.1179/1743284711Y.0000000041
[2] N.A. Belov, A.N. Alabin, I.A. Matveeva, D.G. Eskin: Trans. Nonferrous Met. Soc. China 25 (2015) 2817. DOI:10.1016/S1003-6326(15)63907-3
[3] M.M. Makhlouf, H.V. Guthy: J. Light Met. 1 (2001) 199. DOI:10.1016/s1471-5317(02)00003-2
[4] M. Javidani, D. Larouche: Int. Mater. Rev. 59 (2014) 132. DOI:10.1179/1743280413y.0000000027
[5] S.W. Choi, Y.M. Kim, K.M. Lee, H.S. Cho, S.K. Hong, Y.C. Kim, C.S. Kang, S. Kumai: J. Alloys Compd. 617 (2014) 654. DOI:10.1016/j.jallcom.2014.08.033
[6] M.T. Di Giovanni, E. Cerri, D. Casari, M. Merlin, L. Arnberg, G.L. Garagnani: Metall. Mater. Trans. A 47 (2016) 2049. DOI:10.1007/s11661-016-3366-1
[7] A.R. Farkoosh, X. Grant Chen, M. Pekguleryuz: Mater. Sci. Eng. A 620 (2014) 181. DOI:10.1016/j.msea.2014.10.004
[8] S.K. Shaha, F. Czerwinski, W. Kasprzak, J. Friedman, D.L. Chen: Metall. Mater. Trans. A 46 (2015) 3063. DOI:10.1007/s11661-015-2880-x
[9] K.E. Knipling, D.C. Dunand, D.N. Seidman: Int. J. Mater. Res. 97 (2006) 246.
[10] J. Rakhmonov, G. Timelli, F. Bonollo: Adv. Eng. Mater. 18 (2016) 1096. DOI:10.1002/adem.201500468
[11] S.K. Shaha, F. Czerwinski, W. Kasprzak, J. Friedman, D.L. Chen: Thermochim. Acta. 595 (2014) 11. DOI:10.1016/j.tca.2014.08.037
[12] S.K. Shaha, F. Czerwinski, W. Kasprzak, D.L. Chen: Mater. Des. 59 (2014) 352. DOI:10.1016/j.matdes.2014.02.060
[13] J. Hernandez-Sandoval, G.H. Garza-Elizondo, A.M. Samuel, S. Valtiierra, F.H. Samuel: Mater. Des. 58 (2014) 89. DOI:10.1016/j.matdes.2014.01.041
[14] D. Stefanescu: Casting, Vol. 15, ASM International (1988).
[15] M. Tupaj, A.W. Orlowicz, M. Mroz, A. Trytek, O. Markowska: Arch. Foundry Eng. 16 (2016) 125. DOI:10.1515/afe-2016-0063
[16] T. Gao, D. Li, Z. Wei, X. Liu: Mater. Sci. Eng. A 552 (2012) 523. DOI:10.1016/j.msea.2012.05.081
[17] H.A. Elhadari, H.A. Patel, D.L. Chen, W. Kasprzak: Mater. Sci. Eng. A 528 (2011) 8128. DOI:10.1016/j.msea.2011.07.018
[18] U.M.J. Boin, M. Bertram: JOM. 57 (2005) 26. DOI:10.1007/s11837-005-0022-4
[19] W. Kasprzak, B.S. Amirkhiz, M. Niewczas: J. Alloys Compd. 595 (2014) 67. DOI:10.1016/j.jallcom.2013.11.209
[20] A.R. Farkoosh, X. Grant Chen, M. Pekguleryuz: Mater. Sci. Eng. A 627 (2015) 127. DOI:10.1016/j.msea.2014.12.115
[21] J.G. Kaufman, E.L. Rooy: Aluminum Alloy Castings: Properties, Processes, and Applications, ASM International, Materials Park (2004).
[22] G. Timelli, G. Camicia, S. Ferraro, R. Molina: Met. Mater. Int. 20 (2014) 677. DOI:10.1007/s12540-014-4013-2
[23] D. Casari, M. Merlin, G.L. Garagnani: J. Mater. Sci. 48 (2013) 4365. DOI:10.1007/s10853-013-7252-6
[24] J. Rakhmonov, G. Timelli, F. Bonollo: Mater. Charact. 128 (2017) 100. DOI:10.1016/j.matchar.2017.03.039
[25] P. Sepehrband, R. Mahmudi, F. Khomamizadeh: Scripta Mater. 52 (2005) 253. DOI:10.1016/j.scriptamat.2004.10.025
[26] J. Rakhmonov, G. Timelli, F. Bonollo: Metall. Mater. Trans. A 47 (2016) 5510. DOI:10.1007/s11661-016-3716-z
[27] J. Rakhmonov, G. Timelli, F. Bonollo, L. Arnberg: Int. J. Metalcast. (2016) 1. DOI:10.1007/s40962-016-0076-9
[28] E. Sjolander, S. Seifeddine: J. Mater. Process. Technol. 210 (2010) 1249. DOI:10.1016/j.jmatprotec.2010.03.020
[29] J. Barrirero, J.H. Li, M. Engstler, N. Ghafoor, P. Schumacher, M. Oden, F. Mücklich: Scr. Mater. 117 (2016) 16. DOI:10.1016/j.scriptamat.2016.02.018
[30] H.M. Medrano-Prieto, C.G. Garay-Reyes, C.D. Gómez-Esparza, I. Estrada-Guel, J. Aguilar-Santillan, M.C. Maldonado-Orozco, R. Martínez-Sánchez: Mater. Charact. 120 (2016) 168. DOI:10.1016/j.matchar.2016.08.020
[31] S. Capuzzi, G. Timelli, A. Fabrizi, F. Bonollo, in 7th International Light Metals Technology Conference, LMT 2015, July 27, 2015 – July 29, 2015. (Trans Tech Publications Ltd, Port Elizabeth, South africa, 2015), vol. 828–829, pp. 212–218.
[32] S. Shankar, Y.W. Riddle, M.M. Makhlouf: Metall. Mater. Trans. A 35 (2004) 3038. DOI:10.1007/s11661-004-0048-1
[33] Y.J. Li, A.M.F. Muggerud, A. Olsen, T. Furu: Acta Mater. 60 (2012) 1004. DOI:10.1016/j.actamat.2011.11.003
[34] M. Tocci, R. Donnini, G. Angella, A. Pola: Mater. Charact. 123 (2017) 75. DOI:10.1016/j.matchar.2016.11.022
[35] H.W. Huang, B.L. Ou: Mater Design. 30 (2009) 2685. DOI:10.1016/j.matdes.2008.10.012
[36] A.M.A. Mohamed, F.H. Samuel, S. Al Kahtani: Mater. Sci. Eng. A 577 (2013) 64. DOI:10.1016/j.msea.2013.03.084
[37] A.M.A. Mohamed, F.H. Samuel: in Heat Treatment – Conventional and Novel Applications, Ed.: F. Czerwinski, InTech (2012). DOI:10.5772/50282

[38] E. Rincon, H.F. Lopez, M.M. Cisneros, H. Mancha: Mater. Sci. Eng. A 519 (2009) 128. DOI:10.1016/j.msea.2009.05.022
[39] Q.G. Wang, C.H. Caceres, J.R. Griffiths: Metall. Mater. Trans. A 34 (2003) 2901. DOI:10.1007/s11661-003-0190-1
[40] W.H. Hunt, J.R. Brockenbrough, P.E. Magnusen: Scr. Metall. Mater. 25 (1991) 15. DOI:10.1016/0956-716X(91)90346-3
[41] M. Zamani, S. Seifeddine, A.E.W. Jarfors: Mater. Des. 86 (2015) 361. DOI:10.1016/j.matdes.2015.07.084
[42] G. Rajaram, S. Kumaran, T.S. Rao: Mater. Sci. Eng. A 528 (2010) 247. DOI:10.1016/j.msea.2010.09.020
[43] S.Z. Lu, A. Hellawell: Metall. Trans. A 18 (1987) 1721. DOI:10.1007/BF02646204
[44] T. Gao, X. Liu: J. Mater. Sci. Technol. 29 (2013) 291. DOI:10.1016/j.jmst.2013.01.018
[45] D. Casari, T.H. Ludwig, M. Merlin, L. Arnberg, G.L. Garagnani: Mater. Sci. Eng. A 610 (2014) 414. DOI:10.1016/j.msea.2014.05.059
[46] Y. Sun, S.P. Pang, X.R. Liu, Z.R. Yang, G.X. Sun: Trans. Nonferrous Met. Soc. China 21 (2011) 2186. DOI:10.1016/S1003-6326(11)60993-X
[47] A.K. Dahle, K. Nogita, S.D. McDonald, C. Dinnis, L. Lu: Mater. Sci. Eng. A 413 (2005) 243. DOI:10.1016/j.msea.2005.09.055

(Received April 12, 2018; accepted July 23, 2018)

Correspondence address

Dr. Jovid Rakhmonov
Formerly at Department of Management and Engineering
University of Padova
Stradella S. Nicola, 3 I-36100 Vicenza
Italy
Currently at Department of Applied Sciences
University of Quebec at Chicoutimi
555, Boulevard de l'Université
Chicoutimi, QC G7H2B1
Canada
E-mail: jovid.rakhmonov1@uqac.ca

Bibliography
DOI 10.3139/146.111718
Int. J. Mater. Res. (formerly Z. Metallkd.)
109 (2018) E; page 1 – 14

ISSN 1862-5282